Electronic Supplementary Material (ESI) for Soft Matter.

Supplementary Information for:

Diffusive Dynamics of Nanoparticles in Ultra-confined Media

Jack Deodato C. Jacob[a], Kai He[a], Scott Retterer[b], Ramanan Krishnamoorti[a], and Jacinta C. Conrad[a]

[a]*Department of Chemical and Biomolecular Engineering, University of Houston, Houston, TX 77204-4004*

[b]*Center for Nanophase Materials Sciences and BioSciences Divisions, Oak Ridge National Laboratory, Oak Ridge, TN, 37934*

A. Fabrication of cylindrical nanopost arrays

Nanopost arrays were fabricated using the techniques described by Choi *et al*.[1] ZEP520A photoresist was spin-coated on a 4 in. *p*-type silicon wafer <100> at 6000 rpm for 45 s and baked at 180 °C for 2 min. Square arrays with 0.5 μm circles were produced by e-beam lithography (JBX-9300 FS). The post patterns were then developed in xylene for 30 s, rinsed with isopropyl alcohol (IPA), and dried with N_2. Chromium (15 nm) was deposited using a dual gun electron beam evaporation vacuum chamber (Thermionics, Port Townshend, WA) at a metal evaporation rate of 1 Å/s. The wafer was sonicated in acetone for 10 min to lift off the photoresist and ensure that chromium was only present on the etched surface. Using photolithography, microfluidic channels were fabricated around the nanoposts. Wafers were spin-coated with a negative tone photoresist, NFR016D255cP (JSR Micro Inc., Sunnyvale, CA), at 6000 rpm for 45 s. After baking at 90°C for 90 s, the wafers were aligned to the microchannel optical mask and exposed to ultraviolet light for 3 s. After a post-exposure bake at 115°C for 90 s, the resist was developed in MICROPOSIT MF CD-26 Developer (Shipley Company, Marlboro, MA) for 30 s. After rinsing with DI water and drying with N_2, the wafer was heated on a hot plate at 180 °C for 3 min. The wafers were then cryogenically etched using SF_6 and O_2 at -110°C using an Oxford Plasmalab system 100 to produce 10-μm high nanopost arrays. Finally, a uniform 10 nm thick SiO_2 layer was deposited by atomic layer deposition.

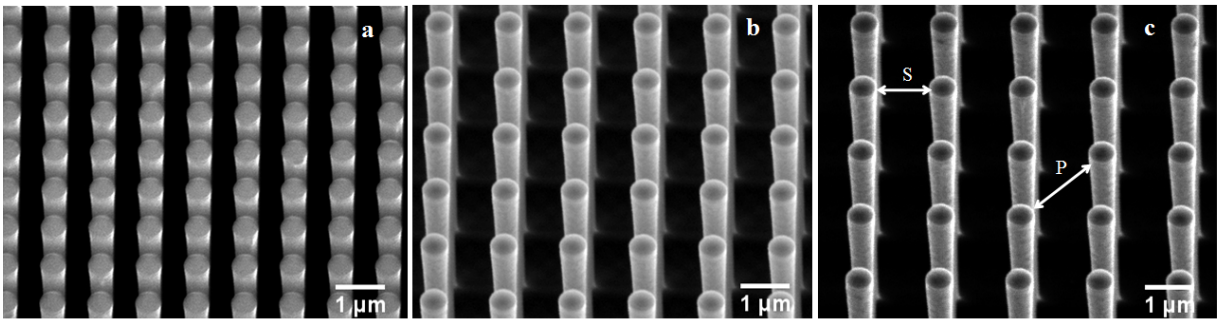

Figure S1. Scanning electron micrographs of the 500 nm-diameter cylindrical post arrays with post spacings of (a) 0.4 μm, (b) 0.8 μm, and (c) 1.0 μm. *S* denotes the spacing between posts while *P* denotes the diagonal of the square post array.

B. Dynamic Differential Microscopy

In differential dynamic microscopy, developed by Cerbino and coworkers[2, 3] a time series of optical microscopy images is analyzed in Fourier space; this method can quantify the dynamics of particles that are too small to be directly resolved by an optical microscope. Differential images were obtained by subtracting microscopy images taken at a fixed time interval Δt. This subtraction eliminated any time-independent signals and revealed a small-scale signal associated with the motion of the particles. The intensity of this signal increased with Δt:

$$D(x,y;\Delta t) = I(x,y;t + \Delta t) - I(x,y;t) \quad (1)$$

where I(x,y;t) is the intensity at position (x,y) measured at time t. A 2D fast Fourier transform of the differential images was performed to obtain the Fourier power spectrum, $D(u_x,u_y;\Delta t)$. If the dynamics are isotropic, the 2-D power spectrum can be azimuthally averaged to obtain the image structure function, D(q, Δt), where $q = 2\pi\sqrt{u_x^2 + u_y^2}$. To determine whether the dynamics were isotropic, azimuthal averaging was done along arc lengths of ±15° orientated parallel to and perpendicular to the nanoposts, as shown in Figures S.2 – S.4. The excellent agreement between

all image structure functions confirmed that the dynamics of nanoparticles in these arrays were isotropic.

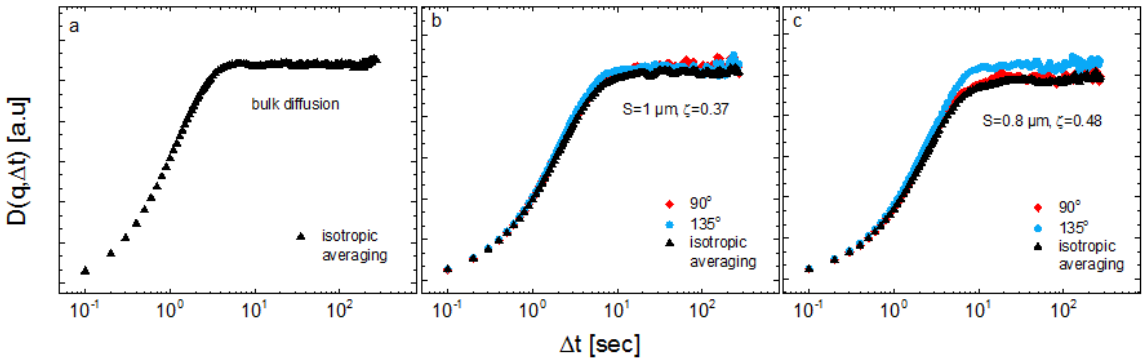

Figure S2. Image structure function D(q, Δt) as a function of delay time Δt at q = 1 μm^{-1} for 400 nm diameter particles (a) diffusing freely and in two different post arrays: (b) S = 1.0 μm and (c) S = 0.8 μm. Black triangles represent particles travelling between posts, red diamonds represent particles diffusing toward the posts, and blue circles represent the isotropic average of the particles.

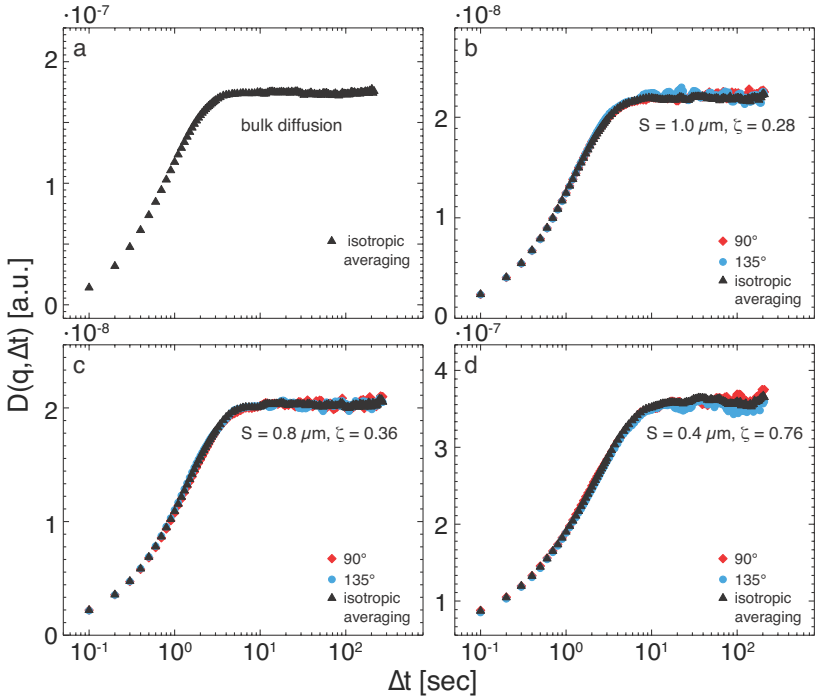

Figure S3. Image structure function D(q, Δt) as a function of delay time Δt at q = 1 μm^{-1} for 300 nm diameter particles (a) diffusing freely and in three different post arrays: (b) S = 1.0 μm (c) S = 0.8 μm, and (d) S = 0.4 μm. Black triangles represent particles traveling between posts, red diamonds represent particles diffusing toward the posts, and blue circles represent the isotropic average of the particles.

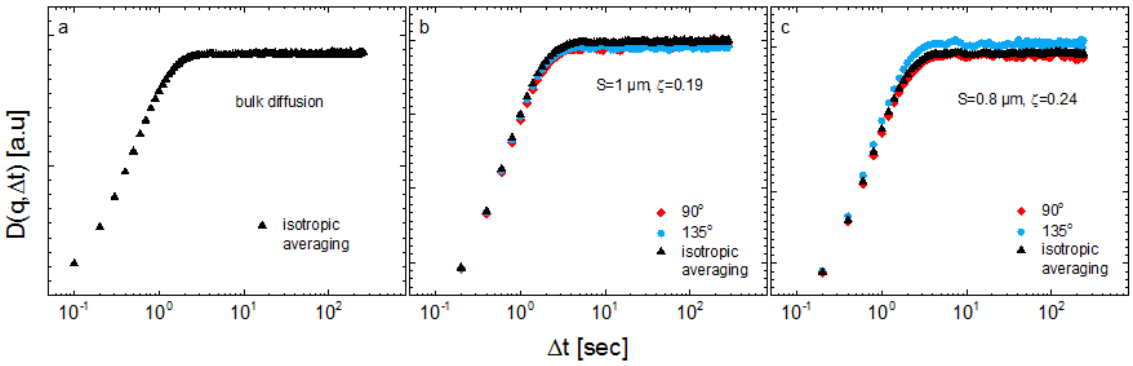

Figure S4. Image structure function D(q, Δt) as a function of delay time Δt at q = 1 μm^{-1} for 200 nm diameter particles (a) diffusing freely and in two different post arrays: (b) S = 1.0 μm and (c) S = 0.8 μm. Black triangles represent particles traveling between posts, red triangles represent particles diffusing toward the posts, and blue circles represent the isotropic average of the particles.

The image structure function (ISF) of particles diffusing in bulk could be fitted using a simple exponential model,

$$D(q,\Delta t) = A(q)\left[1 - \exp\left(-\frac{\Delta t}{\tau(q)}\right)\right] + B(q) \quad (2)$$

where A(q) is the signal prefactor, which depends on the scattering properties of the particles, the light source and the system optics; B(q) is the background noise of the system; and τ(q) is the q-dependent relaxation time. Non-linear least-squares fitting was performed using the Levenberg-Marquardt algorithm in Origin software (OriginLab, Northampton, MA). Three parameters were extracted from the fitting: A(q), B(q), and τ(q). The particle diffusivity D_m was then calculated from the slope of τ(q) versus q^2 as $Dm = 1/\tau(q)q^2$. A(q) and B(q) are shown for representative experiments in Figures S5 – S7; we note that B(q) is nearly constant over all wave vectors accessed in these experiments, despite the presence of the posts.

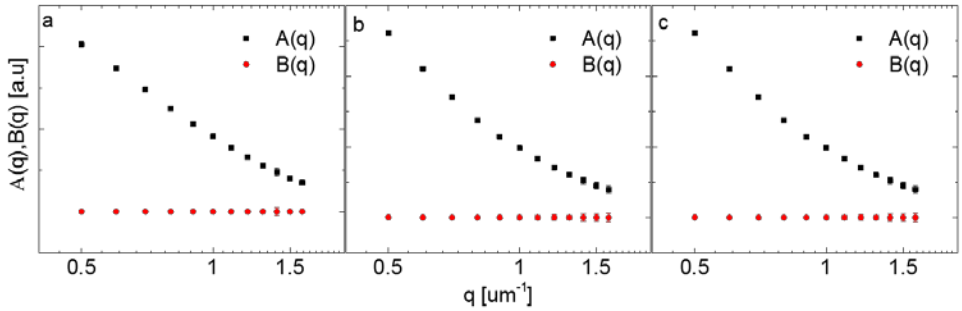

Figure S5. Fitting parameters A(q) (black squares) and B(q) (red circles) as a function of the magnitude of the wave vector q (in μm^{-1}) of 200 nm particles a.) diffusing freely and in post arrays with b.) S=0.8 μm, c.) S=1.0 μm.

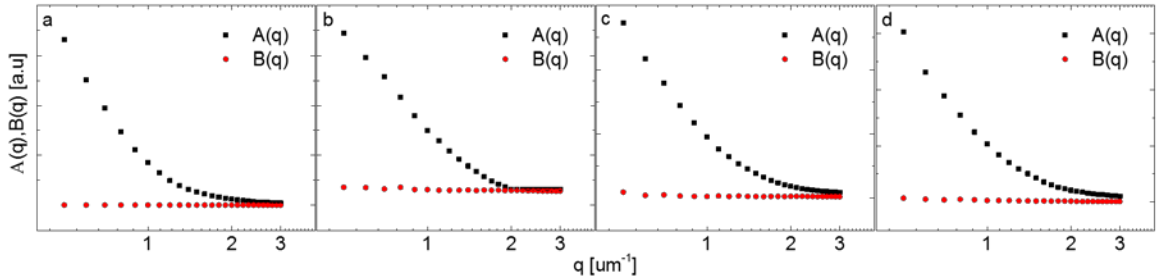

Figure S6. Fitting parameters A(q) (black squares) and B(q)) (red circles) as a function of the magnitude of the wave vector q (in μm^{-1}) of 300 nm particles a.) diffusing freely and in post arrays with b.) S=0.8 μm, c.) S=1.0 μm, and d.) S=2.0 μm.

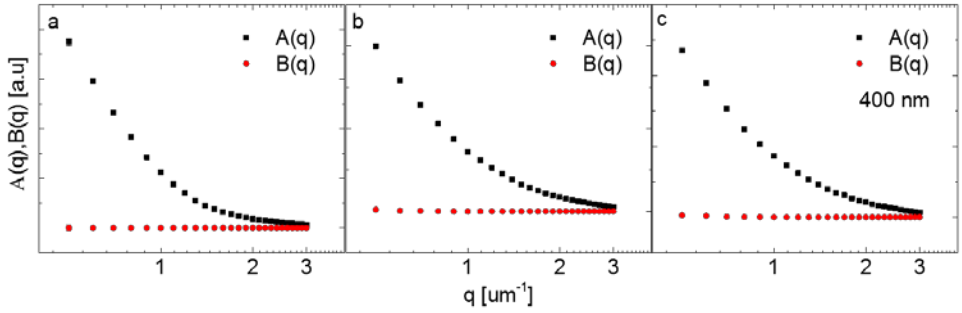

Figure S7. Fitting parameters *A(q)* (black squares) and *B(q)* (red circles) as a function of the magnitude of the wave vector q (in μm^{-1}) of 200 nm particles a.) diffusing freely and in post arrays with b.) S=0.8 μm, c.) S=1.0 μm.

As shown in Figure S8, the ISF of 400 nm particles diffusing in bulk with wave vectors below 3 μm^{-1} could be fitted using Equation 2. Figures S9 and S19 show that Equation 2 could also be applied to fit the ISFs of freely diffusing 300 and 200 nm particles, respectively.

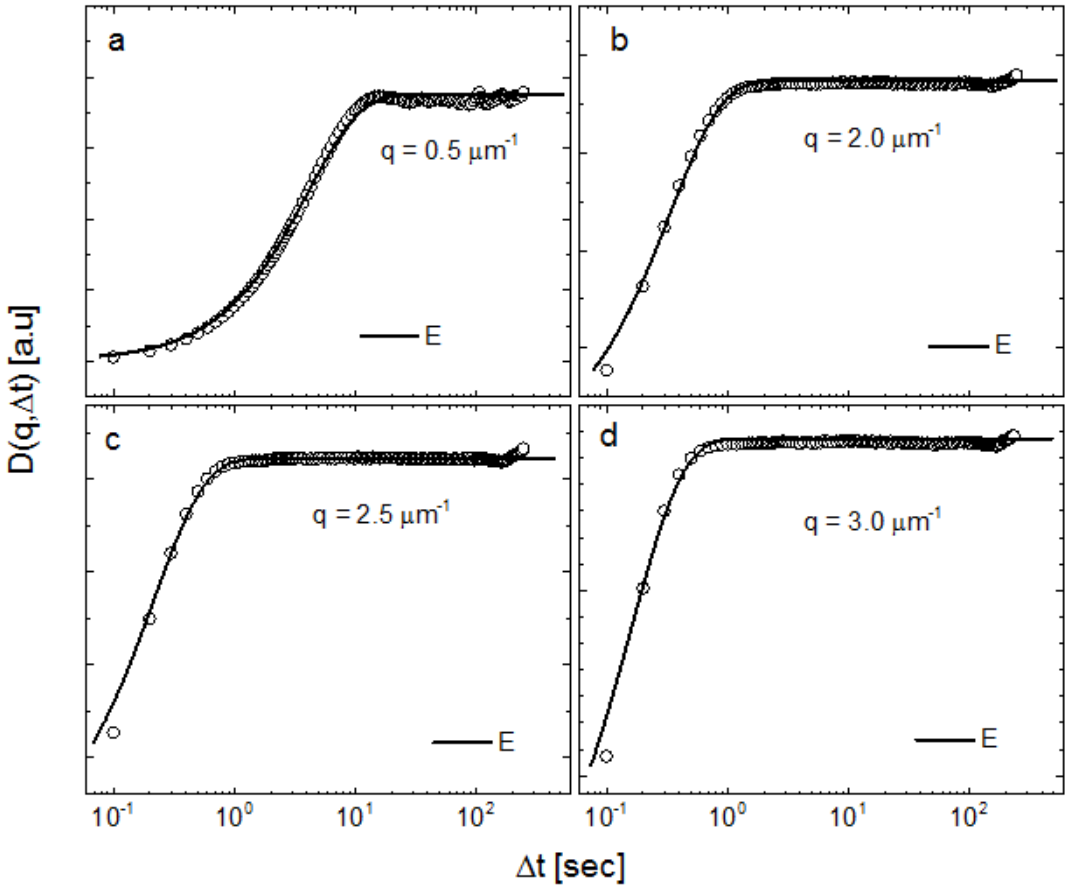

Figure S8. Image structure function D(q,Δt) of 400 nm particles diffusing in bulk at different wave vectors: (a) 0.5 μm^{-1}, (b) 2.0 μm^{-1}, (c) 2.5 μm^{-1}, and (d) 3.0 μm^{-1}.

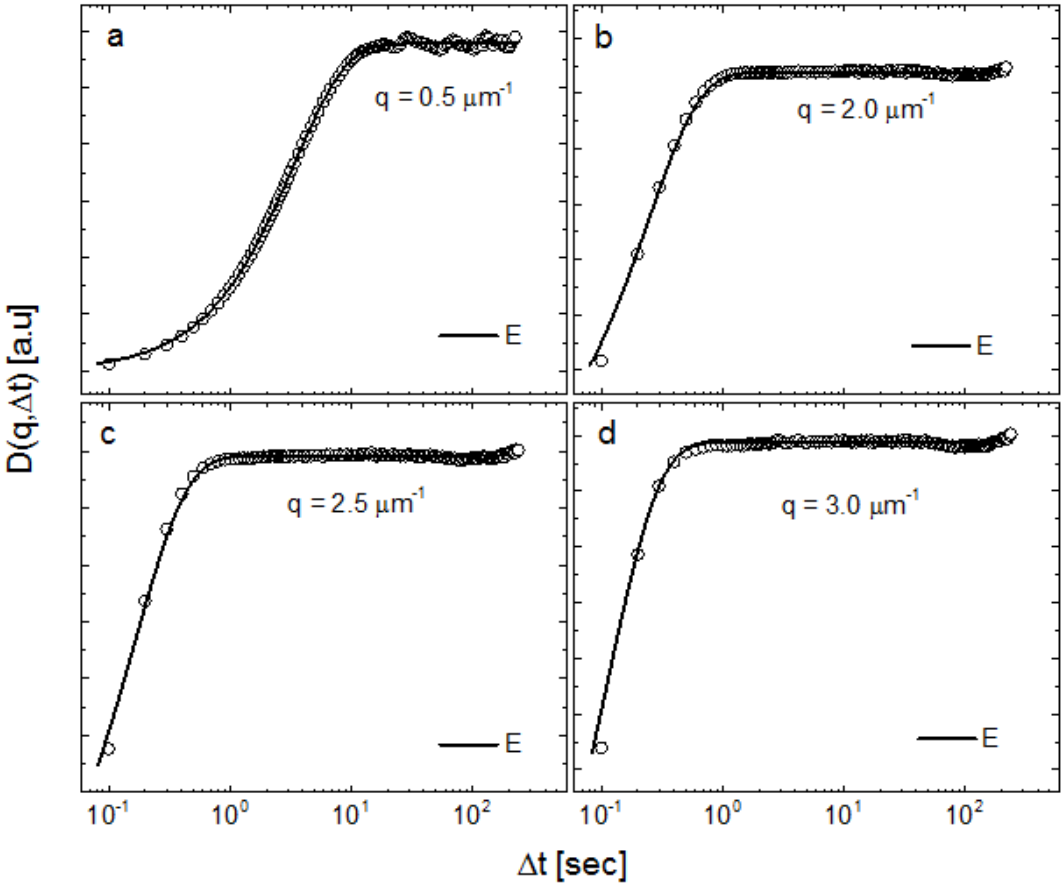

Figure S9. Image structure function D(q,Δt) of 300 nm particles diffusing in bulk at different wave vectors: (a) 0.5 μm^{-1}, (b) 2.0 μm^{-1}, (c) 2.5 μm^{-1}, and (d) 3.0 μm^{-1}.

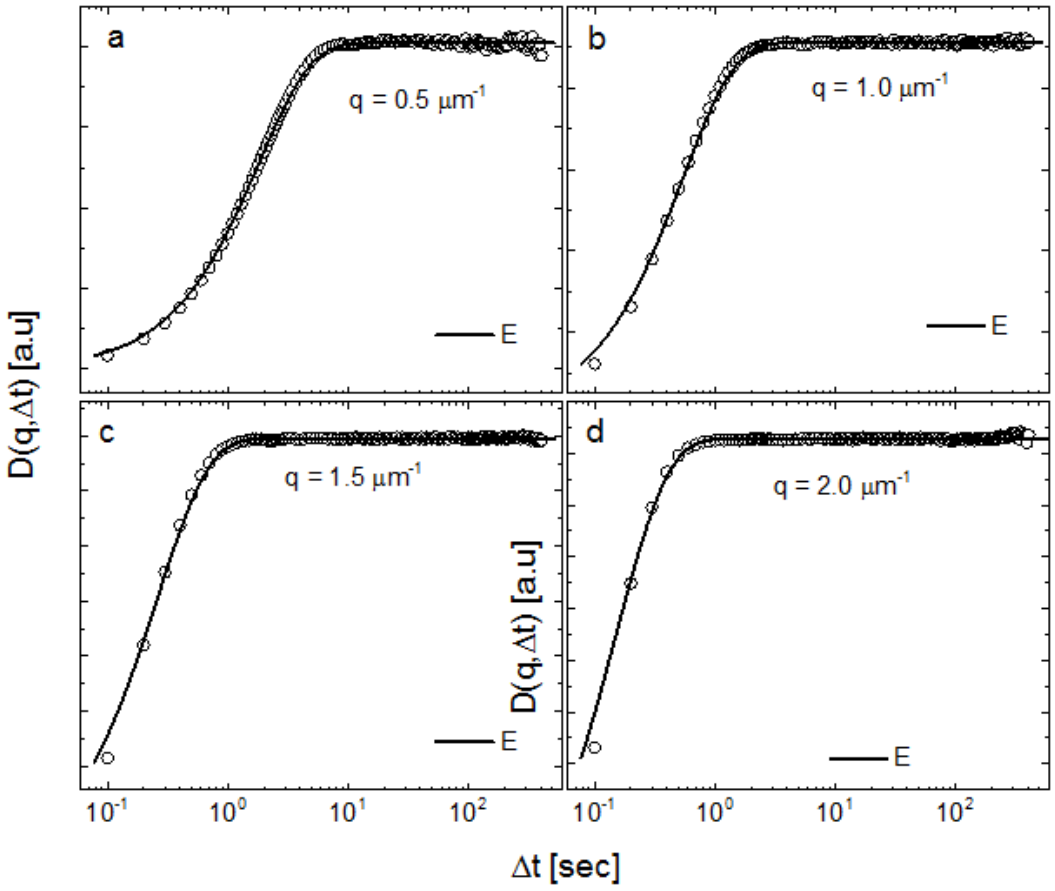

Figure S10. Image structure function D(q,Δt) of 200 nm particles diffusing in bulk at different wave vectors: (a) 0.5 μm^{-1}, (b) 1.0 μm^{-1}, (c) 1.5 μm^{-1}, and (d) 2.0 μm^{-1}.

The dynamics of particles diffusing in confined nanopost arrays, however, cannot be fitted using Equation 2. Instead, these dynamics were fitted using a stretched exponential model,

$$D(q,\Delta t) = A(q)\left[1 - \exp\left(-\frac{\Delta t}{\tau(q)}\right)^{r(q)}\right] + B(q) \quad (3)$$

where r(q) is the stretching exponent.

We found that r(q) was nearly independent of q at wave vectors below 2 μm^{-1}. At higher wave vectors, r(q) decreased as q was increased. To test the robustness of the fitting equation, the ISFs of nanoparticles diffusing in nanoposts were fitted multiple times with different parameters.

The first fitting allowed r(q) to vary from 0 to 1 and an average value was obtained from the low q-range where r(q) is nearly constant. The ISFs were fitted again with this average r(q). Figures S11 – S17 show the ISFs of nanoparticles at different wave vectors fitted using different values of r(q).

The ISFs of 400 nm particles diffusing in post arrays with S=1 μm were fitted using an r(q) of 0.92 from wave vectors 0.5 to 2.0 μm^{-1}. At q = 2.5 μm^{-1}, r(q) decreased to 0.83 and further decreased to 0.77 at q = 3.0 μm^{-1} (Figure S11). We observed that r(q) had a significant effect on fitting at q values less than 2 μm^{-1}. Figure S12 shows that 400 nm particles diffusing in post arrays with S=0.8 μm follow the same trend.

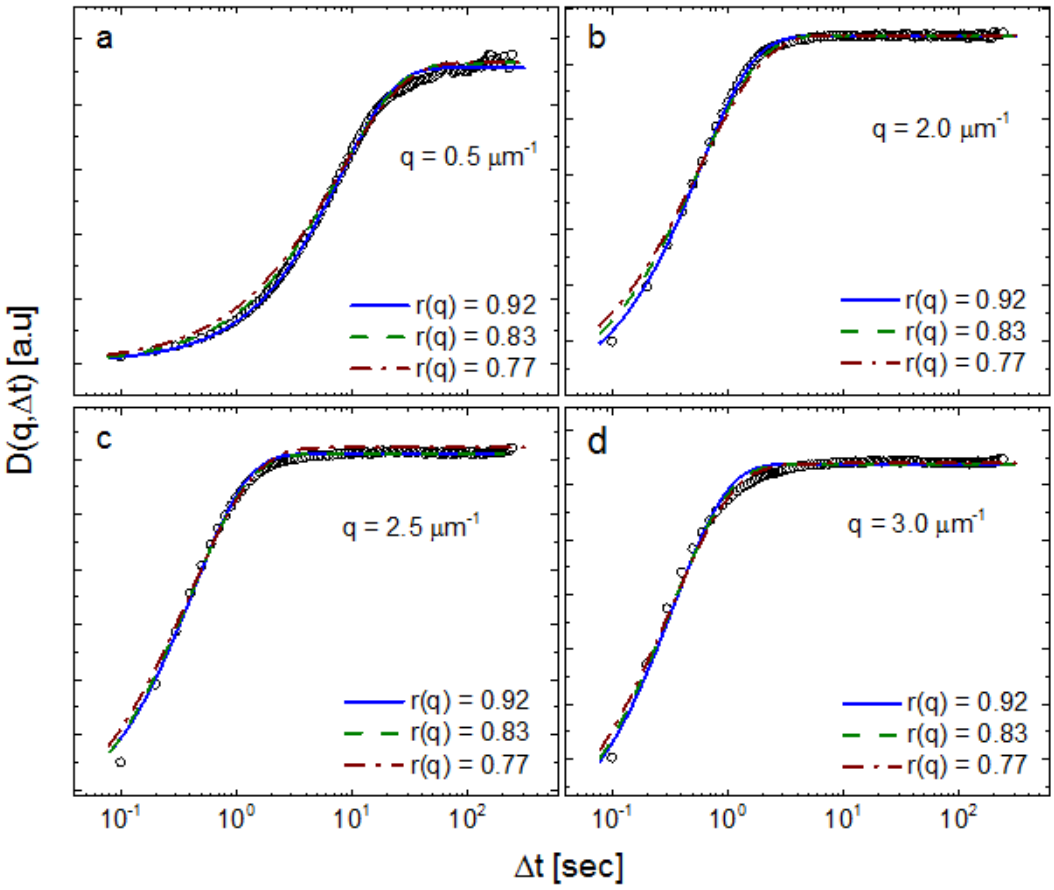

Figure S11. Image structure function D(q,Δt) of 400 nm particles diffusing in post arrays with S=1 μm fitted with different stretching exponents r(q) at different wave vectors: (a) 0.5 μm^{-1}, (b) 1.0 μm^{-1}, (c) 2.5 μm^{-1}, and (d) 3 μm^{-1}.

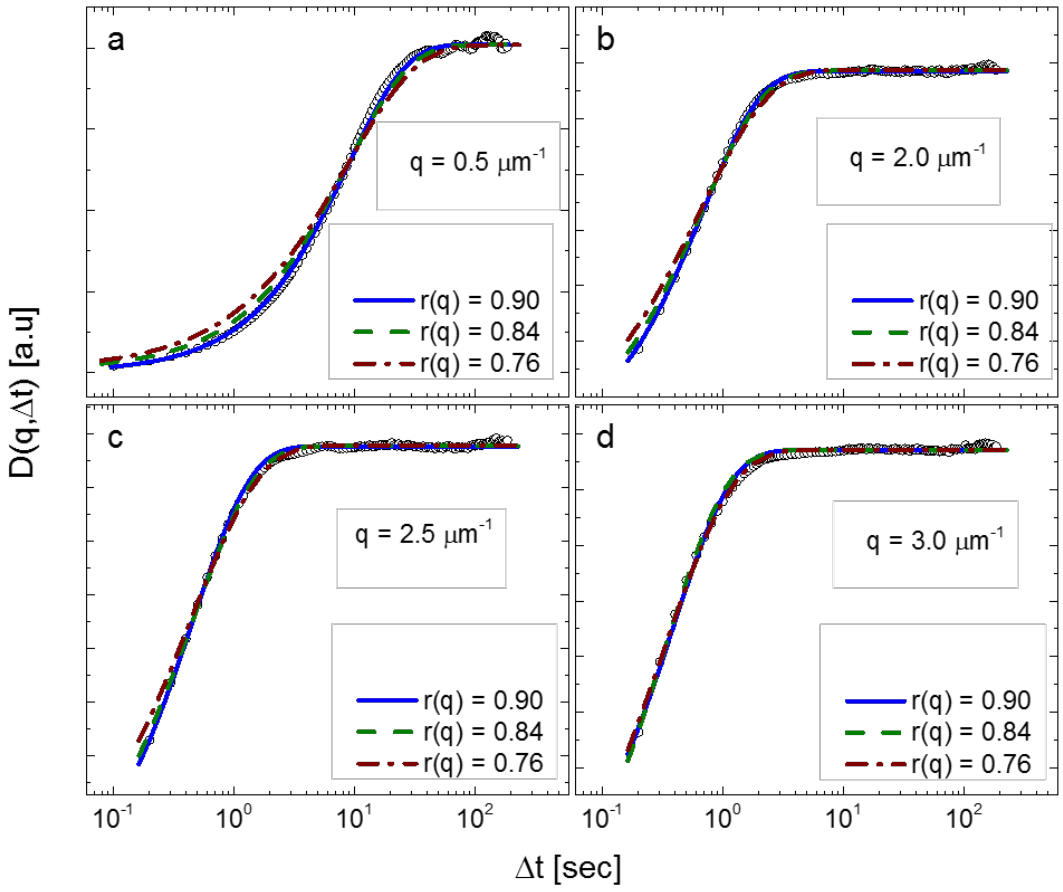

Figure S12. Image structure function D(q,Δt) of 400 nm particles diffusing diffusing in post arrays with S=0.8 μm fitted with different stretching exponents r(q) at different wave vectors: (a) 0.5 μm^{-1}, (b) 1.0 μm^{-1}, (c) 2.5 μm^{-1}, and (d) 3 μm^{-1}.

For 300 nm particles diffusing in post arrays with S=1 μm, an average r(q) value of 0.92 was extracted from the ISFs from wave vectors 0.5 to 2 μm^{-1}. Above that range the r(q) values decreased as q increased until a r(q) of 0.63 was derived from q = 3 μm^{-1}. Figure S13 shows that changing the r(q) value had a significant effect on the ISF fitting over the q range of 0.5 – 3 μm^{-1}. As shown in Figures S14 and S15, this was not the case for 300 nm particles diffusing in post

arrays with S=0.8 and 0.4 μm, respectively. In those systems, the fitting was sensitive to r(q) at wave vectors less than 2 μm^{-1}, but became less sensitive at higher wave vectors.

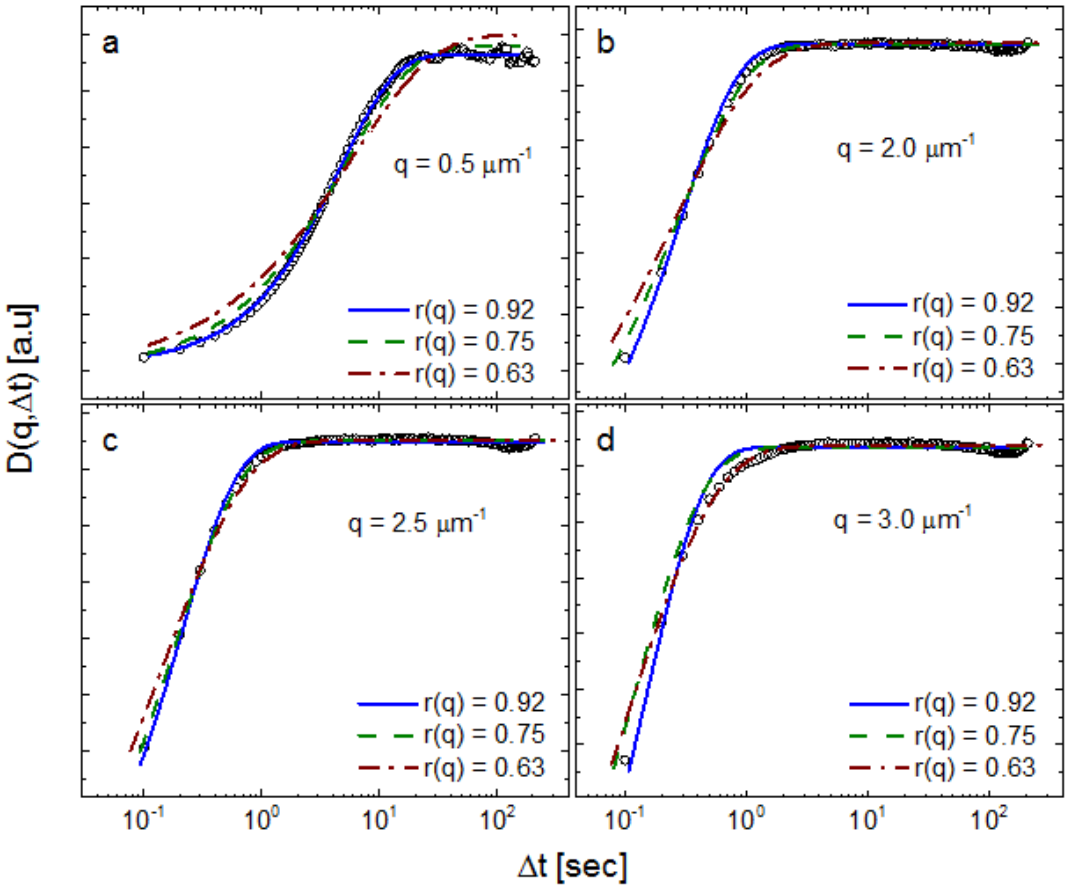

Figure S13. Image structure function D(q,Δt) of 300 nm particles diffusing in post arrays with S=1 μm fitted with different stretching exponents r(q) at different wave vectors: (a) 0.5 μm^{-1}, (b) 1.0 μm^{-1}, (c) 2.5 μm^{-1}, and (d) 3 μm^{-1}.

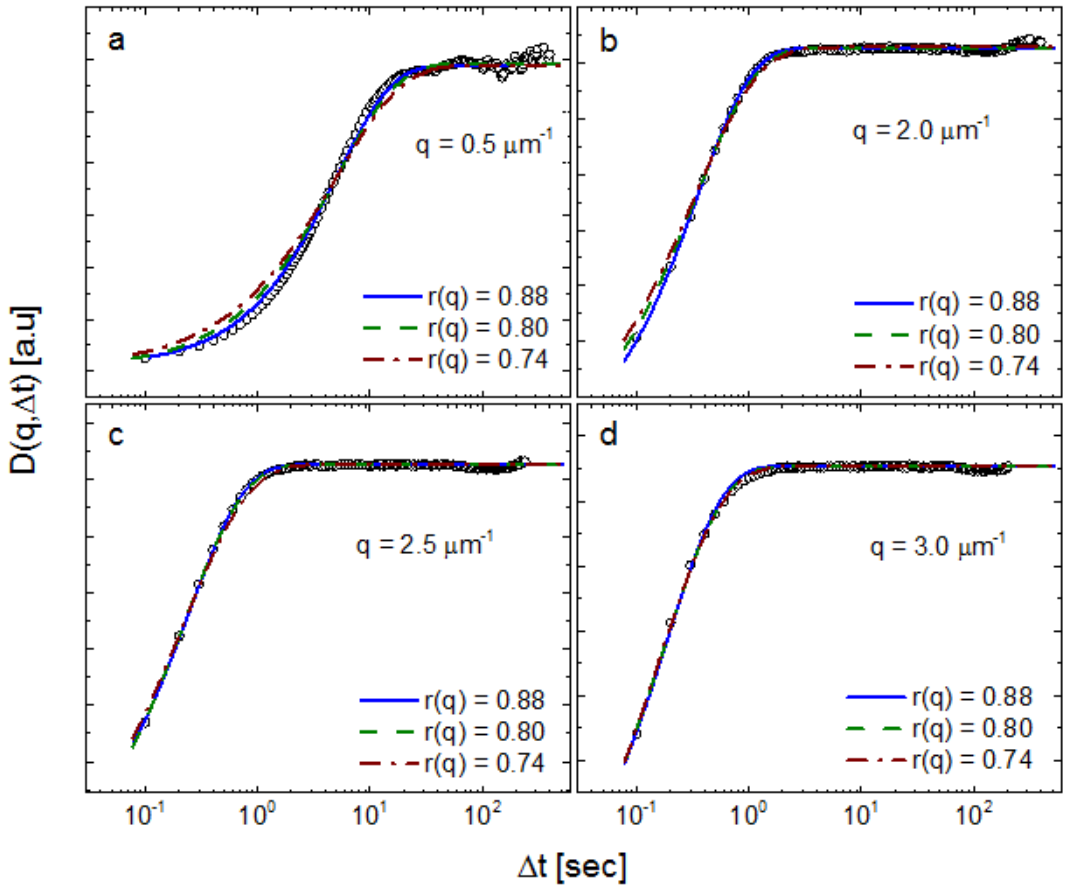

Figure S14. Image structure function D(q,Δt) of 300 nm particles diffusing in post arrays with S=0.8 μm fitted with different stretching exponents r(q) at different wave vectors: (a) 0.5 μm^{-1}, (b) 1.0 μm^{-1}, (c) 2.5 μm^{-1}, and (d) 3 μm^{-1}.

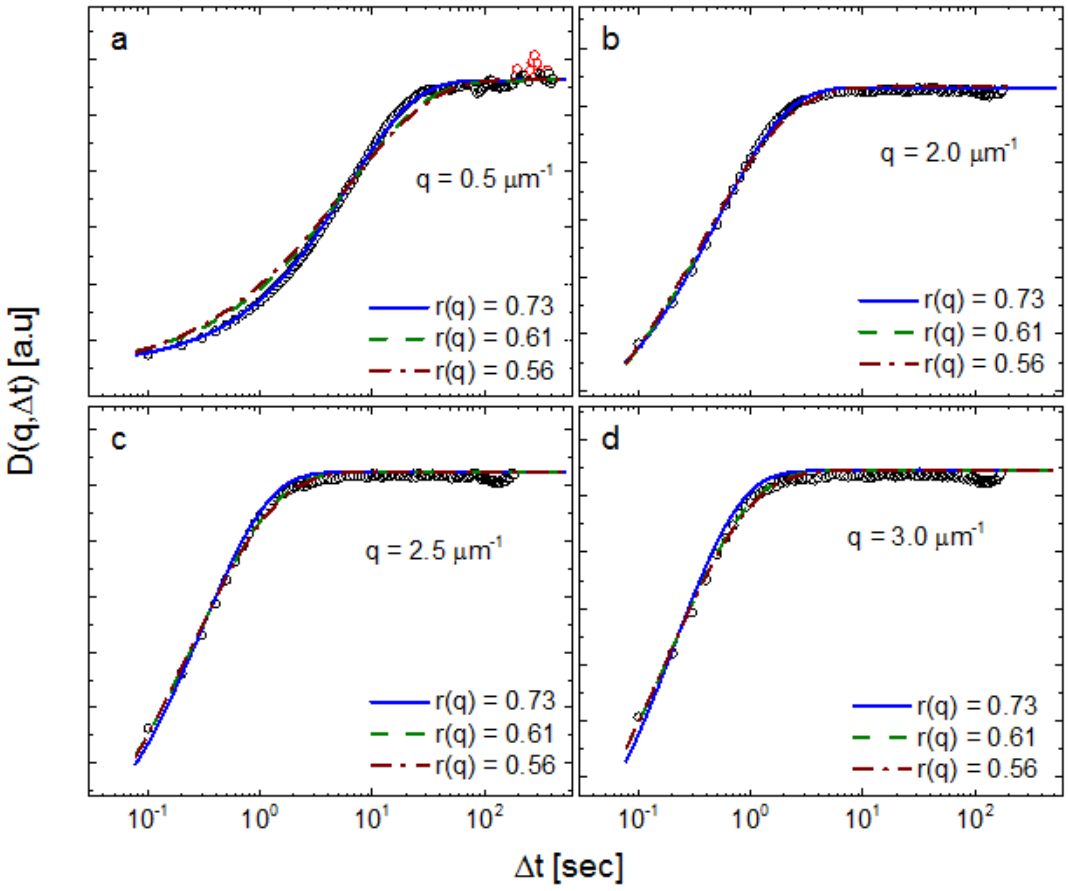

Figure S15. Image structure function D(q,Δt) of 300 nm particles diffusing in post arrays with S=0.4 μm fitted with different stretching exponents r(q) at different wave vectors: (a) 0.5 μm^{-1}, (b) 1.0 μm^{-1}, (c) 2.5 μm^{-1}, and (d) 3 μm^{-1}.

The ISFs of 200 nm particles diffusing in post arrays with S=1 μm and S=0.8 μm are shown in Figures S16 and S17, respectively. The average r(q) could be used to fit ISFs for wave vectors ranging from 0.5 to 2.0 μm^{-1}.

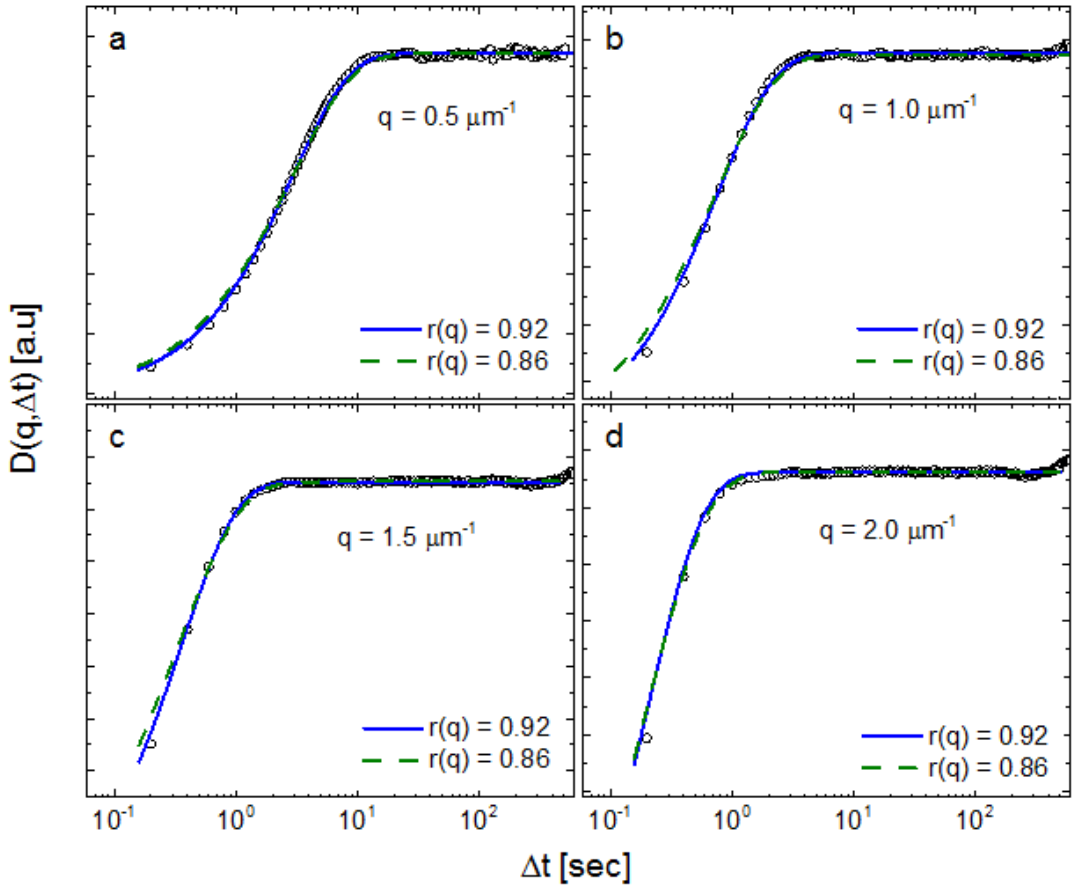

Figure S16. Image structure function D(q,Δt) of 200 nm particles diffusing in post arrays with S=1 μm fitted with different stretching exponents r(q) at different wave vectors: (a) 0.5 μm^{-1}, (b) 1.0 μm^{-1}, (c) 1.5 μm^{-1}, and (d) 2 μm^{-1}.

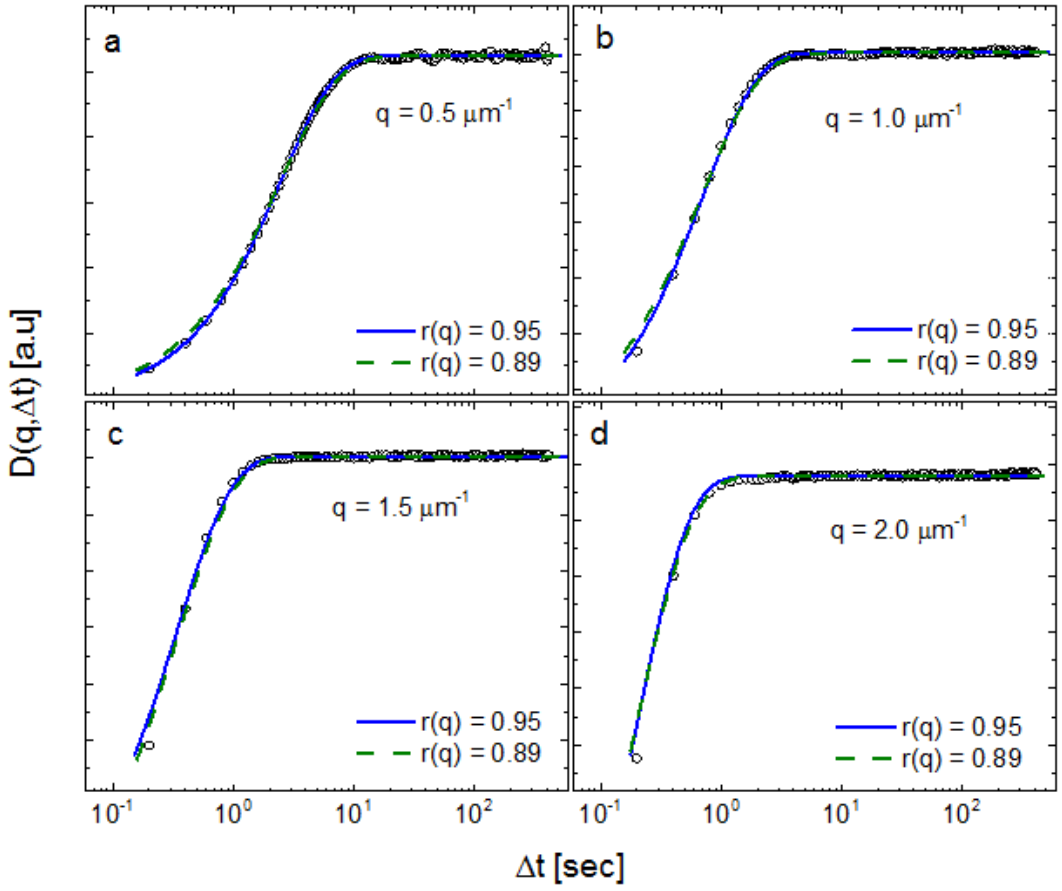

Figure S17. Image structure D(q,Δt) of 200 nm particles diffusing in post arrays with S=0.8 μm fitted with different stretching exponents r(q) at different wave vectors: (a) 0.5 μm^{-1}, (b) 1.0 μm^{-1}, (c) 1.5 μm^{-1}, and (d) 2 μm^{-1}.

Table S1. Wave vector q at which the stretching exponent r(q) begins to deviate from its small-q average for the different particle sizes and post spacings investigated in this study.

Nanoparticle diameter [nm]	**q value for which $r(q) < 0.95\langle r(q)\rangle$ [μm^{-1}]**		
	Post spacing [nm]		
	400	**800**	**1000**
300	2.0 ± 0.2	2.2 ± 0.2	2.0 ± 0.2
400	-	2.6 ± 0.2	2.4 ± 0.2

Table S1 shows the approximate wave vector at which $r(q)$ (Figure 4 in the main manuscript) begins to deviate from the average value $\langle r(q) \rangle$. For the different post spacings explored in this study and for the two sizes of particles for which we observe a deviation, the deviation wave vector ranges from 2.0 – 2.6 μm^{-1}, corresponding to length scales of 2.4 – 3.1 μm. Given the limited range of data, no systematic understanding is possible.

The relaxation time $\tau(q)$ did not significantly depend on the value of $r(q)$ used to fit the ISFs. Figures S18 – S21 show that fixing $r(q)$ to its average value or allowing $r(q)$ to vary produced fits with equivalent $\tau(q)$ values within the errors associated with the measurements.

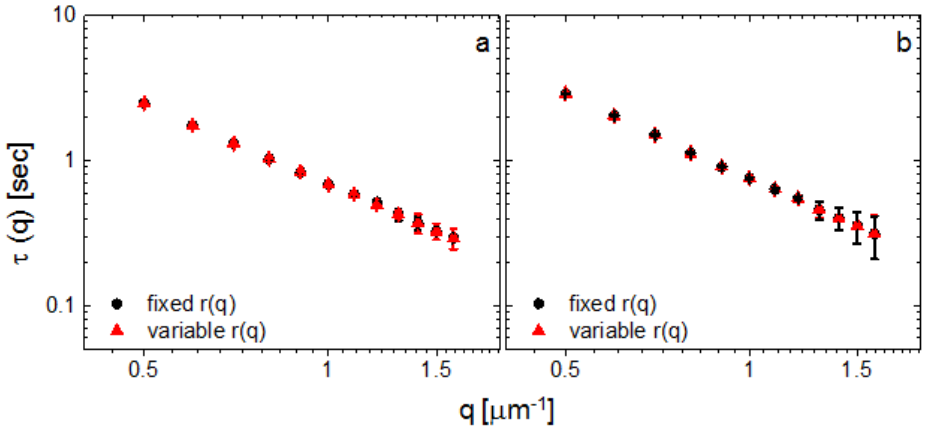

Figure S18. Relaxation time τ(q) (in seconds) as a function of the magnitude of the wave vector q (in μm^{-1}) for 400 nm nanoparticles diffusing in post arrays with (a) S=1 μm, with r(q) fixed at 0.92 and r(q) varied from 0.77 – 0.92 and (b) S=0.8 μm, with r(q) fixed at 0.90 and r(q) varied from 0.76 – 0.90.

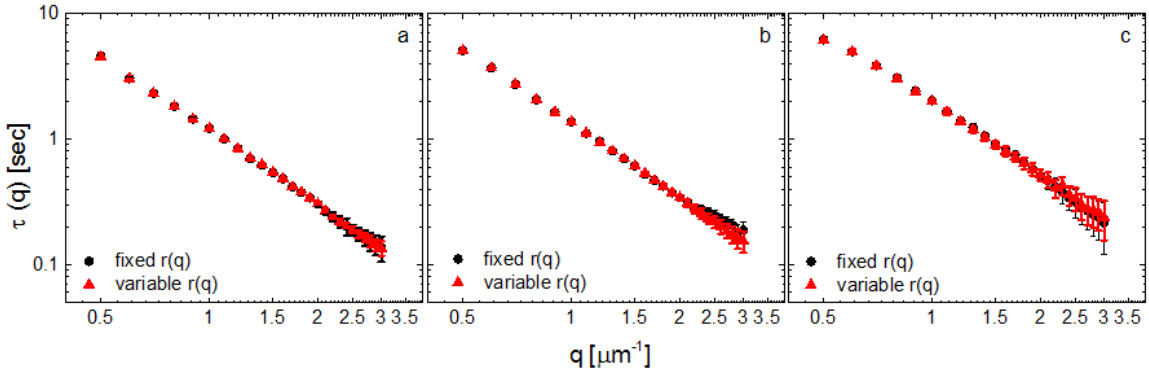

Figure S19. Relaxation time τ(q) (in seconds) as a function of the magnitude of the wave vector q (in μm^{-1}) 300 nm nanoparticles diffusing in post arrays with (a) S=1 μm, with r(q) fixed at 0.92 and r(q) varied from 0.63 – 0.92, (b) S=0.8 μm, with r(q) fixed at 0.89 and r(q) varied from 0.74 – 0.89, and (c) S=0.4 μm, with r(q) fixed at 0.73 and r(q) svaried from 0.56 – 0.73.

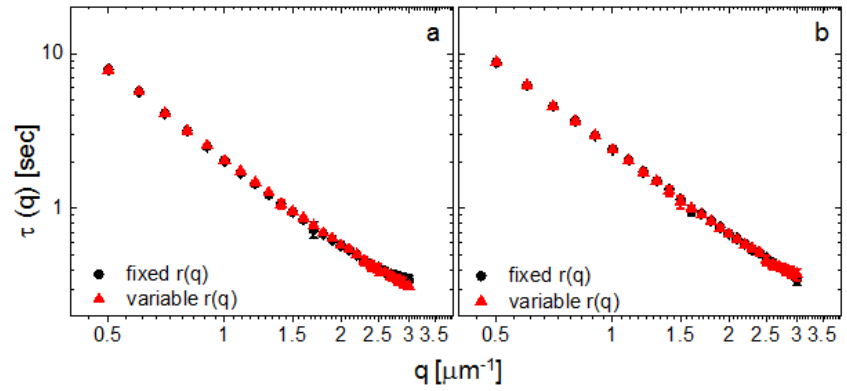

Figure S20. Relaxation time τ(q) (in seconds) as a function of the magnitude of the wave vector q (in μm^{-1}) 200 nm nanoparticles diffusing in post arrays with (a) S=1 μm, with r(q) fixed at 0.95 and r(q) varied from 0.89 – 0.95, (b) S=0.8 μm, with r(q) fixed at 0.92 and r(q) varied from 0.86 – 0.92.

Particle trajectories obtained using a single particle-tracking (SPT) algorithm were analyzed to validate the diffusivities obtained using DDM. Centroids were located to within 40 nm and particle positions were linked into trajectories. The mean square displacement (MSD) of the particles was calculated from the trajectories using Equation 4 and the probability distributions of particle displacements were computed using Equation 5.

$$\left\langle \Delta x^2(\Delta t) \right\rangle = \left\langle \left(\Delta x^2(t+\Delta t) - x(t) \right)^2 \right\rangle \quad (4)$$

$$G(\Delta x, \Delta t) = C_1 \exp\left[-\left(\frac{|\Delta t|}{\gamma(\Delta t)} \right)^{\beta} \right] + C_2 \exp\left[-\left(\frac{\Delta t}{\lambda} \right)^2 \right] \quad (5)$$

Here C_1 and C_2 are prefactors and g(Δt) and λ are the decay lengths for stretched and simple Gaussians, respectively. In our previous study, we found that the displacement distributions for nanoparticles deviated from a simple Gaussian and were instead fitted with a sum of a simple and stretched Gaussian model.[4] To fit these distributions, β was set to 2r(q) (derived from DDM) and λ was set to a constant width.

The MSD of the 400 nm particles diffusing freely and through the nanopost arrays are shown in Figure S21. The MSDs exhibited the same trend with increasing confinement, consistent with the slowing of dynamics observed in DDM. The diffusion coefficients extracted from the MSD were identical to those obtained using DDM within the errors of each measurement, as shown in Table S1.

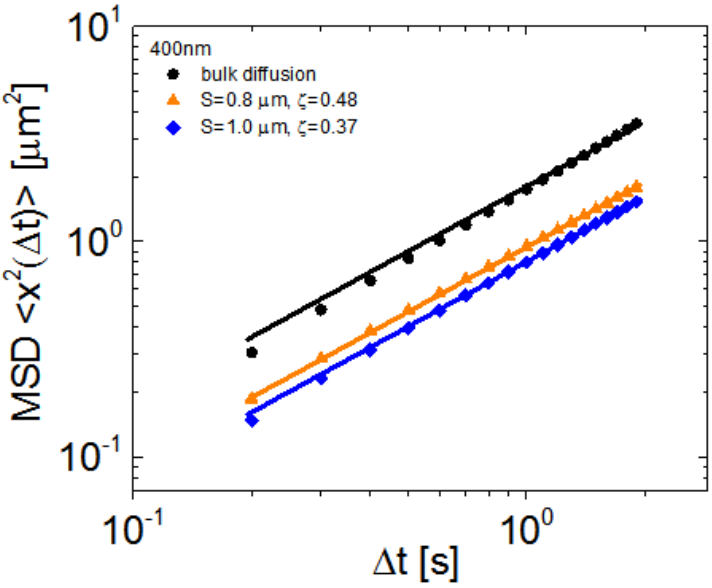

Figure S21. Mean-squared displacement (MSD) as a function of delay time Δt for 400 nm nanoparticles diffusing freely (black circles) and in post arrays with S= 0.8 µm, ζ=0.48 (orange triangles) and S=1.0 µm, ζ=0.37 (blue diamonds). The MSD scales linearly with Δt across the range of delay times probed.

The one-dimensional distributions of displacements ($G_s(\Delta x, \Delta t)$) fitted to Equation 5 are shown in Figure S22. The decay lengths extracted from the fits decreased as particles were increasingly confined, as shown in Figure S23. This decay length represented the average characteristic length scale of the processes contributing to the stretched Gaussian distribution. The relative decay lengths (γ/γ_0), where γ_0 is the decay length of freely diffusing particles, are shown in Table S2.

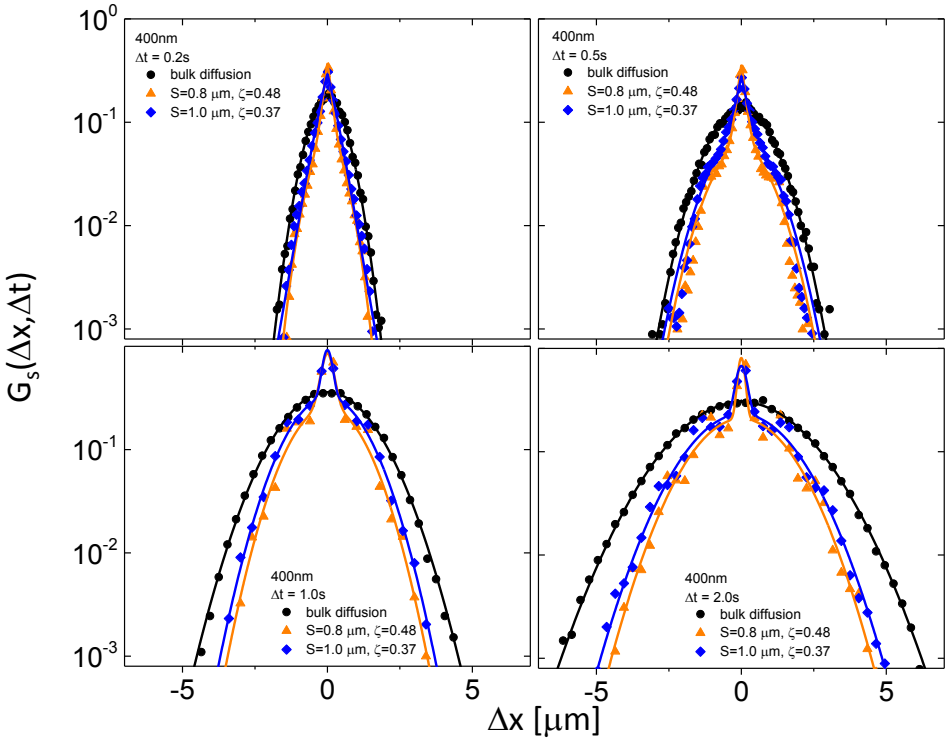

Figure S22. Probability distributions of particle displacements $G_s(\Delta x, \Delta t)$ for 400 nm particles diffusing freely and in post arrays with S=0.8 μm, ζ=0.48, and S=1.0 μm, ζ=0.37, at delay times Δt of (a) 0.2 s, (b) 0.4 s, (c) 0.6 s and (d) 0.8 s, respectively. Lines indicate fits to Equation 5.

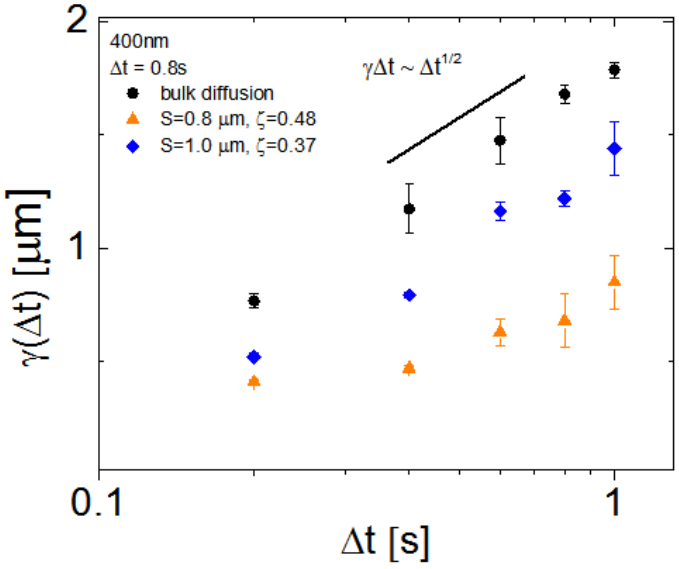

Figure S23. Decay length γ(Δt) as a function of delay time Δt for 400 nm particles diffusing freely (black circles) and in post arrays with S=0.8 μm (orange triangles), ζ=0.48, and S=1.0 μm (blue diamonds), ζ=0.37, respectively.

Table S2. Relative diffusivities, stretching exponents, and relative decay lengths of 400 nm particles diffusing through post arrays measured using DDM and using particle tracking.

Post Spacing	DDM		Particle Tracking	
	Relative Diffusion (D/D_0)	**Stretching Exponent (r(q))**	**Relative Diffusion (D/D_0)**	**Relative Decay Length (γ/γ_0)**
S = 1 μm	0.54 ± 0.03	0.90 ± 0.01	0.55 ± 0.03	0.71 ± 0.03
S = 0.8 μm	0.47 ± 0.03	0.87 ± 0.04	0.46± 0.03	0.63 ± 0.03

References

1. C. K. Choi, J. D. Fowlkes, S. T. Retterer, P. Siuti, S. Iyer and M. J. Doktycz, *ACS Nano*, 2010, **4**, 3345-3355.
2. R. Cerbino and V. Trappe, *Phys. Rev. Lett.*, 2008, **100**, 188102.
3. F. Giavazzi, D. Brogioli, V. Trappe, T. Bellini and R. Cerbino, *Physical Review E*, 2009, **80**, 031403.
4. K. He, F. Babaye Khorasani, S. T. Retterer, D. K. Thomas, J. C. Conrad and R. Krishnamoorti, *ACS Nano*, 2013, **7**, 5122-5130.